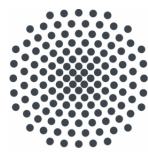


Setting up a lightsheet for realizing quasi two-dimensional quantum gases

Bachelorthesis

Sina Hammer

19th December 2017



University of Stuttgart
Germany

5th Institute of Physics

Examiner: Prof.Dr. Tilman Pfau

Ehrenwörtliche Erklärung

Hiermit versichere ich, dass ich diese Arbeit selbst verfasst habe und nur die angegebenen Quellen verwendet wurden. Alle wörtlich oder sinngemäß aus anderen Werken übernommenen Aussagen sind als solche gekennzeichnet. Die eingereichte Arbeit ist oder war weder als Ganzes, noch in wesentlichen Teilen Gegenstand eines anderen Prüfungsverfahrens und wurde weder vollständig noch in Teilen bereits veröffentlicht. Der Inhalt des gedruckten und elektronischen Exemplars stimmt überein.

Declaration of Authorship

I hereby declare that I wrote this thesis on my own and I did not use any other sources than those referred to. Parts that are quotes or paraphrases of other works are marked as such by indicating the references. This thesis is neither whole nor partly subject of another examination and has not been published elsewhere. The electronic and printout version are identical.

Stuttgart, 19.12.2017

Sina Hammer

Abstract

Deutsch

Im Rahmen dieser Arbeit wurde eine optische Falle in Form eines Lichtblatts zur Realisierung von quasi zwei-dimensionalen ultrakalten Quantengasen konstruiert und deren Fallenfrequenz bestimmt. Diese wird nun in einem Experiment verwendet, dass ein einzelnes Rydbergatom in einem Bose-Einstein-Kondensat beobachtet. Dabei erhofft man sich durch eine nahezu zweidimensionale Atomwolke, eine Erhöhung des Kontrasts der Messungen.

Der dazu entworfene Aufbau besteht aus strahlformenden optischen Elementen sowie einem Regelkreis zu Intensitätsstabilisierung des verwendeten Laserstrahls der Wellenlänge 855 nm. Dieser Regelkreis setzt sich aus einem akusto-optischen Modulator und einem PID-Regler¹ zusammen, deren Funktionsweisen im Rahmen dieser Arbeit beschrieben werden.

Aus dem intensitätsstabilisierten Strahl wurde dann durch zwei Zylinderlinsen und eine sphärische Linse eine Falle mit elliptischer Geometrie geformt. Für die Strahltaillen der Falle ergaben sich Werte von $w_{0,x} = 110.7(\pm 5.9)\mu\text{m}$ entlang der langen Achse und $w_{0,y} = 10.1(\pm 2.0)\mu\text{m}$ entlang der kurzen Achse. Abschließend wurde die Fallenfrequenz des Lichtblatts aus der Messung der Oszillation der gefangenen Atomwolke bestimmt. Dabei konnte eine Frequenz von $f = 1363(\pm 8)$ Hz festgestellt werden.

¹Proportional-Integral-Derivative-Controller

English

In the scope of this bachelor thesis, a lightsheet for realizing quasi two-dimensional ultracold quantum gases was designed. Furthermore, the trap frequency of the lightsheet was measured. The trap is now used at an experiment, which observes a single Rydberg impurity in a Bose-Einstein-Condensate. In this case, working with a nearly two dimensional cloud of atoms should improve the contrast of the measurements.

The designed setup includes a feedback loop for intensity stabilization and the optical setup for shaping the lightsheet. The feedback loop consists of an acousto-optical modulator and a PID-Controller¹. Their basic working principles are described within this thesis. Then, the stabilized beam was shaped via two cylindrical and one spherical lens, to get an elliptical geometry. A Measurement of the beam waist revealed for the short and the long axis $w_{0,x} = 110.7(\pm 5.9)\mu\text{m}$ and $w_{0,y} = 10.1(\pm 2.0)\mu\text{m}$ respectively. Finally, using absorption imaging of the atom cloud's oscillation dynamics, the trap frequency was measured and a frequency of $f = 1363(\pm 8)\text{ Hz}$ was extracted from the data.

¹Proportional-Integral-Derivative-Controller

Contents

1	Motivation	6
2	The Acousto-optical Modulator	7
2.1	Basic Working Principles	7
2.2	Technical Setup	9
2.2.1	AOM-Driver-Box	9
2.2.2	Final Arrangement	11
3	PID-Controller	13
3.1	Basic Working Principle	13
3.1.1	Proportional-Part	14
3.1.2	Integrational-Part	14
3.1.3	Derivative-Part	14
3.2	Technical Setup	15
3.2.1	Modified PID for Intensity Stabilization	15
3.2.2	Final Arrangement of the AOM and the PID to a Feedback Loop	17
4	The Lightsheet	19
4.1	Basic Working Principles	19
4.1.1	Gaussian Optics	19
4.1.2	Optical Traps	20
4.2	Final Setup for the Lightsheet	22
4.3	Quantifying the Trap Frequency of the Lightsheet	25
4.3.1	Theoretical Calculation	25
4.3.2	Analysis of an Exemplary Measurement	27
5	Conclusion and Outlook	29
	Appendix	30
A	AOM	30
B	PID	32
	References	34

Chapter 1

Motivation

The aim of this thesis is to design a light sheet, to realize quasi two-dimensional ultra cold clouds. The constructed trap should then be used at an experimental setup, which observes a single Rydberg impurity in a Bose-Einstein-Condensate. Utilizing the interaction between the Rydberg electron and the BEC¹, the aim of the experiment is to image the orbital of the outer Rydberg electron. The electron orbit can be measured as density changes of the surrounding BEC. Those density changes are caused by the attractive potential of the Rydberg electron. This effect could be visualized, as the surrounding BEC flows like a gas towards the areas of high electron probability density [3].

For this purpose it is favorable to work with a quasi two-dimensional sample to increase the expected contrast. To generate two-dimensional samples, a trap that provides two-dimensional confinement is needed. That is realized by a lightsheet, a trap with an elliptical geometry.

This lightsheet relies on the principle of optical dipole traps, as they can be realized in a great "variety of different trapping geometries"[1]. This thesis outlines how to set up a feedback loop for laser intensity stabilization and construct the beam shaping setup to finally get the deserved trap configuration.

It is necessary to stabilize the intensity of the beam for the lightsheet, to avoid heating of the atom cloud inside the trap. On that account, the basic working principles of an acousto-optical modulator and PID-controller² as parts of the feedback loop are described. Moreover the technical details of the constructed parts are discussed. To understand the working principles of the lightsheet, the basic principles of optical traps are outlined. Moreover, the arrangement of the optical components used to shape the beam is described. Finally, the trap frequency of the lightsheet is specified.

¹Bose-Einstein-Condensate

²Proportional-Derivative-Integrative controller

Chapter 2

The Acousto-optical Modulator

To set up the lightsheet, the intensity of the laser beam must be controlled and stabilized. For this purpose an acousto-optical modulator with a center frequency of 80 MHz is used in combination with a PID controller. In the following sections the basics and the technical realization of the AOM¹ and its driving devices are described.

2.1 Basic Working Principles

The following description of the basic principles of acousto-optical modulators is based on the references [6],[7] and [8].

Acousto-optical modulators can be used for modulating the intensity and frequency, or controlling the spatial direction of a laser beam. An AOM is based on the principle of the acousto-optic effect. This effect describes the diffraction of light through sound waves. It is an effect of photoelasticity, where the medium permittivity changes under mechanical strain [22]. This leads to a change in the refractive index, where the index variation is periodic, with the same wavelength as the acoustic wave.

Basically there are two types of AOMs used, Bragg- and Raman-Nath modulators. This two types, Raman-Nath- and Bragg-diffraction, can be distinguished by the parameter Q which is defined as

$$Q = \frac{2\pi\lambda l}{n\Lambda^2} \quad (2.1)$$

where Λ is the wavelength of the acoustic wave and λ the wavelength of the laser beam. Moreover n is the refractive index of the crystal and l the distance the beam passes through the acoustic wave. For $Q \ll 1$ it is the Raman-Nath-regime and for $Q \gg 1$ the Bragg-regime.

In this setup a modulator based on Bragg-diffraction is used.

The basic scheme of a Bragg-based AOM with an incidence angle Θ_B is shown in Figure 2.1. This incident angle must be greater than zero, to get a diffracted beam. Typically an AOM consists of a transparent crystal, usually a Quartz-Crystal, which is driven by an externally applied radio-frequency. The RF-signal² is coupled to a

¹Acousto-optical Modulator

piezoelectric transducer which excites a soundwave with the frequency of the RF-signal. At the other end of the crystal an absorber avoids reflection to inhibit the occurrence of standing waves. The induced wave propagates in the crystal, creating a 'phase grating'. Any laser beam sent through the crystal will be diffracted by this 'grating', due to Bragg reflection. For that reason AOMs are sometimes also called Bragg cells.

The diffraction pattern of the 'phase grating' could be described with Bragg-deflection following

$$2 \cdot \Lambda \sin(\Theta_B) = \lambda m. \quad (2.2)$$

The parameter m defines the order of the maximum. Because the grating moves through the crystal, the Doppler-Effect must be considered, which leads to a frequency shift at the amount of the acoustic frequency. This effect could also be explained with a view to the behavior of the wave vectors \vec{k} . The conservation of momentum leads to

$$\vec{k}_d = \vec{k}_i \pm \vec{k}_a \quad (2.3)$$

with \vec{k}_d the vector of the diffracted beam, \vec{k}_i of the incident beam and \vec{k}_a of the acoustic wave in the crystal. In addition, based on the energy conservation

$$f_d = f_i \pm f_a \quad (2.4)$$

is given for the frequencies of the waves. The frequency shift f_a is typically between 80 MHz and 2 GHz for common AOMs. If the frequency of the laser is in- or decreased depends on the propagation direction of the sound wave relative to the laser beam. For $\Theta_B < 0$ the frequency is decreased, for $\Theta_B > 0$ it is increased. The optical power in the diffracted beam can be controlled via the acoustic power.

Depending on the incident angle, the first or the minus first diffraction order is more intense. With a well adjusted angle also the second, third or higher orders can be made visible. At the proper angle most of the power is in the diffracted beam, amounts of 80 to 90% of the power of the incident beam are achievable.

²Radio-Frequency-signal

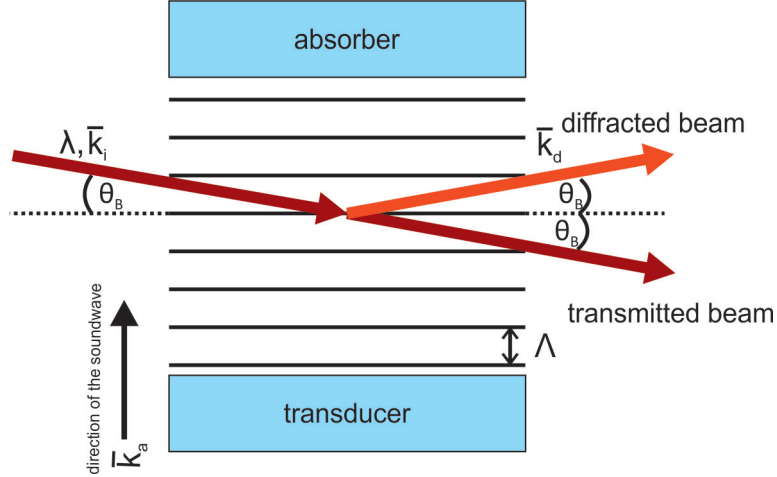


Figure 2.1: Scheme of the Bragg-diffraction inside the AOM, based on [6]. The incident beam (dark-red) is diffracted at the phase grating induced by the soundwave. Due to Bragg-Diffraction the incident angle equals the diffraction angle.

2.2 Technical Setup

2.2.1 AOM-Driver-Box

The acousto-optical modulator is controlled with a self-built radio-frequency driver-box. This box is needed to generate a suitable signal to apply to the AOM. The modulator type used in this experiment requires a 80 MHz signal with a minimum power of 1.5 W (= 31.76 DBm) to work efficiently [9]. This signal is created by a self-built AOM-Driver-Box, basically constructed according to the scheme in Figure 2.2, [5]. The main element is a DDS-Board¹ which generates the signal for operating the AOM. Because the signal, directly picked up from the boards output, has not enough power (≈ -7 dBm), it has to be amplified. For that reason the box contains an amplifier circuit to increase the amplitude of the signal. Moreover the signal should also be fast disengageable, which is realized with a TTL switch, included to the amplifier circuit. Figure 2.2 shows the basic connections of the driver box.

The box includes a four channel AD9959 Evaluation Board (DDS-Board) manufactured by Analog Devices [10], working as a frequency synthesizer. This board generates a signal at the desired frequency. It could operate with the internal reference clock or with an optional addable crystal as reference. For this setup a voltage controlled oscillator with a frequency of 25 MHz is used. The board is controlled from a computer via USB and the related evaluation board software. The frequency, amplitude and phase of each channel can be controlled separately. Based on the requirements of the used AOM (Crystal technologies, type 3080-125) [9], the frequency of the corresponding channel of the DDS-Board is set to 80 MHz.

The Filter-Out output of the board is connected to the **L**-connector of a MiniCircuit ZP-1LH-S+ mixer [11] with SMA cables. The **X**-pin of the mixer is connected to the front panel electronics and provided with a control current of less than 30 mA.

¹direct digital synthesis

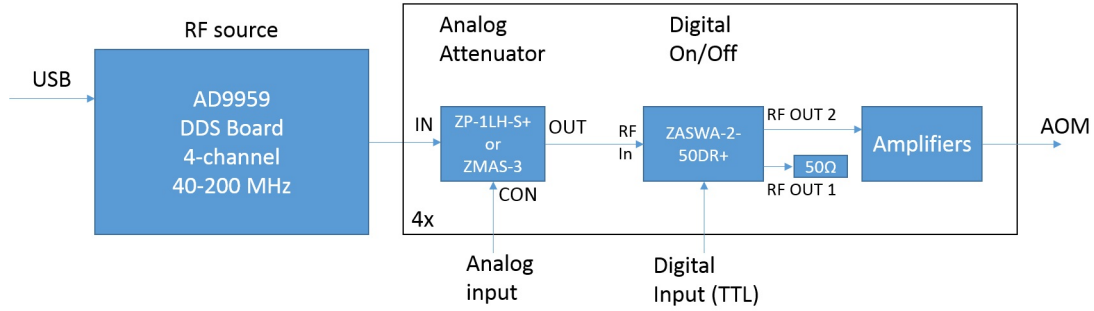


Figure 2.2: Scheme of the main components of the AOM-Driver-Box. The signal is generated with the DDS-Board and then amplified by the circuit in the right black box. *Source:*[5]

This current is depending on the voltage applied to the power connector at the front panel electronics. Their circuit diagram is shown in Figure A.1 in the appendix. The mixer then multiplies the signal from the board with the applied control current. Through that, the mixer decreases the power of the signal.

In the next step, the signal passes through a MiniCircuit ZASWA-2 – 50DR+ switch [12]. The **R**-output of the upstream mixer is connected with the RF input of the switch. Also the TTL input is connected to a BNC-pin on the front panel and an applied signal operates the switch. The switch has two RF outputs, RF output one is terminated with 50Ω , because the switch can only operate between the two channels, not between on and off. When RF output two is on, the signal passes, when output one is on, it's blocked. At this configuration for TTL 'high' RF output two is activated, for TTL 'low' RF output one is activated.

After the switch the signal passes a pre-amplifier ZX60-6013E-S+ from MiniCircuits [13] and then a bigger amplifier ZHL-3A-S+ [14], to increase the output power of the signal. Depending on the power needed for the AOM the amplifiers could be varied.

Figure 2.3 shows the output signal of the Box measured at a frequency of 30 MHz, where the amplitude of the signal is increased to 38 dBm, by the amplifiers. The performance of this configuration is shown in 2.4. The ideal frequency range is up to 80 MHz, there high amplifying is achievable. This box should not be operate over 150 MHz, which is the max. input frequency of the ZHL-3A-S+ amplifiers. Otherwise they could be damaged. Moreover the outputs of the amplifiers always have to be terminated with 50Ω , when a signal is applied, otherwise they could be damaged through reflection.

The self-designed power supply circuit is shown in Figure A.2 in the appendix. This board supplies the 1.8 V and 3.3 V for the DDS board and the 12 V for the smaller amplifiers. The bigger amplifiers are directly powered with 24 V. Also the switches have to be powered with ± 5 V. For that the circuit in Figure A.3 in the appendix is designed. Both circuits A.2 and A.3 are built on one board together, as the 12 V for the TRACO TEN5-1221 DC/DC Converter [15] in Picture A.3 could be picked up from the 12 V generated in circuit A.2.

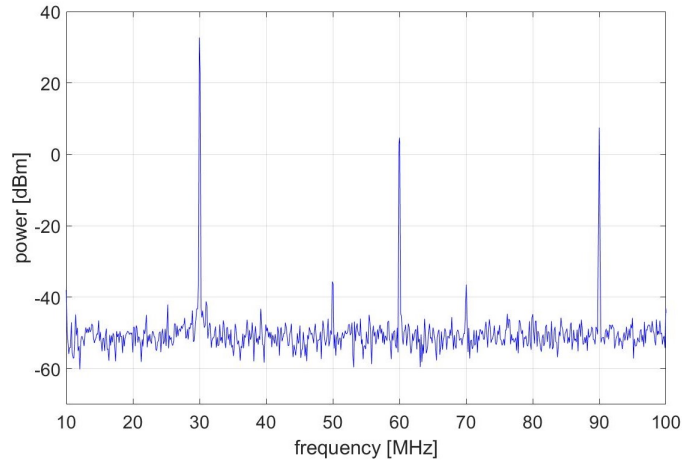


Figure 2.3: Output power signal of the driver box operating at 30 MHz, measured with an oscilloscope. Besides the peak at 30 MHz, peaks at the multiples 60 MHz and 90 MHz are visible.

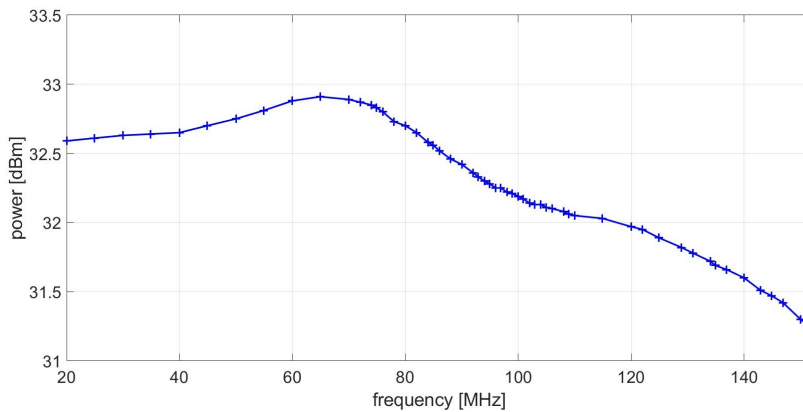


Figure 2.4: Performance of the output of the AOM-driver-box. The output power is showed versus the frequency.

2.2.2 Final Arrangement

Primarily, different types of AOMs were tested. Finally, a Crystal Technology AOM Model 3080-125 is in use. This modulator has a center frequency of 80 MHz and a bandwidth of 25 MHz. The polarisation is 90° to the mounting base and the Bragg angle is 6 mrad. In the experiment it operates at 80 MHz. The data sheet shows diffraction efficiencies up to 93% for wavelengths of 633 nm, depending on the beam diameter [9]. With the used wavelength of 855 nm, an efficiency up to 80% is viable. This AOM is operated with the driver box described above. For the experiment the minus first diffraction order is used.

As shown in Picture 2.5, the 855 nm laser beam was picked up with a polarizing beam splitter right after the output of the laser. Then the beam was sent through a telescope, built of a $f = 100$ mm and a $f = -50$ mm lense to get a suitable beam waist for the input to the AOM. Afterwards, the beam was sent through the AOM

with an adjustable mirror in front, for the alignment. The output beams of the AOM then passed a $\lambda/2$ -waveplate and a polarizing beamsplitter. Right before the fiber coupler the first order diffracted beam was separated from the other orders with an iris. The fiber guided the modulated beam to another experiment table, where the first setup for the stabilization and later on for the lightsheet were tested before including them to the original experiment table.

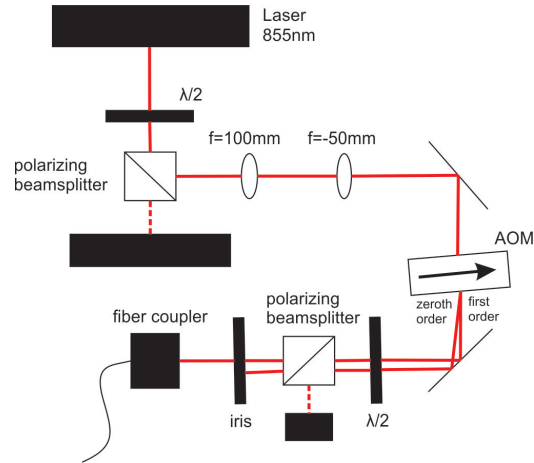


Figure 2.5: Sketch of the final setup for the intensity modulation, including the AOM. After the beam is modulated, the first diffraction order is coupled in a fiber.

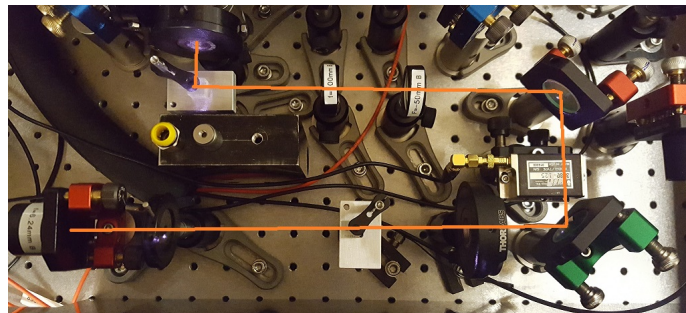


Figure 2.6: Picture of the setup as it is built in the experiment. Two adjustable mirrors are necessary for adjusting the path of the beam through the AOM and the fiber coupling.

Chapter 3

PID-Controller

An AOM on its own can control the frequency or intensity of the diffracted laser beam, but can not hold it exactly stable. However, for the lightsheet it is important that the intensity which reaches the atom cloud does not fluctuate. Disturbances could be caused by fluctuations of the intensity leaving the AOM as well as drifts in the fiber coupling. For that reason, in addition to the AOM a PID¹ is necessary, to complete the feedback loop.

In the PID three different controller types are combined to adjust the process value. These three controllers are a Proportional-, an Integrative and a Derivative-Controller. PIDs could be used for different purposes, like frequency or intensity stabilization. In this experiment, the PID is used to stabilize the intensity of the laser beam, diffracted by the AOM, as part of a feedback loop circuit. The following sections describe the basic functions of PIDs based on the references [17] and [22], as well as how a PID for intensity stabilization is designed.

3.1 Basic Working Principle

Basically, the PID compares the current value of the process variable with the desired value and tries to stabilize the current value at the desired level. In this case the process variable is the intensity of the beam, measured in front of the optical setup for generating the lightsheet. The set point defines the value the PID tries to achieve and hold. For that purpose it continuously compares the set point value with the current value and creates an error variable, which is the difference of this two values. If there is a difference between set point and the process variable the error is non-zero. The variable the PID works with is this error variable, its aim is to keep the error permanently zero.

For realizing that, the PID uses three separate controller types in combination. For some purposes it is useful to only use one or two of these controllers, so for most PIDs they can be switched on and off separately. The used design has separately switchable controllers, because for the intensity stabilization especially the P- and I-Parts are necessary. The three different controller types are described each separately in the following paragraphs.

¹Proportional-Integral-Derivative

3.1.1 Proportional-Part

The Proportional-Part multiplies the resulting error variable $e(t)$ with a proportional constant K_p to create the output value $y(t)$

$$y_p(t) = K_p \cdot e(t). \quad (3.1)$$

If the error is equal to zero, the output value is zero too, if it is negative, the output is negative, etc. If solely positive output values are desired, an output offset can be set. In this case the output range is adjusted between 0 and 10 V and the proportional part decreases the output voltage for negative errors and increases it for positive errors. If the error is zero, the output stays at the set voltage which should operate the AOM at the desired amplitude. So, ideally the output of the PID just varies by a small amount in the vicinity of the basic voltage. The amplitude of this part could be increased via a higher proportional constant K_p . However if K_p is too large, the system can start to oscillate as the controller countersteers too strongly. When K_p is adjusted too small, the set point and the output value diverge. If this controller is used without the Integrational-Part, one problem is that it never reaches steady state [17].

3.1.2 Integrational-Part

As the Proportional-Controller always leaves an offset between set point and process variable the I-part is needed.

The Integrative-Controller integrates the error over a period of time and adjusts the output $y_i(t)$ until the error value is zero

$$y_i(t) = K_i \cdot \int_0^t e(\tau) d\tau \quad (3.2)$$

This eliminates the steady state error from the P-Part [17]. If the error value reaches a negative level it increases the output value or decreases it for a positive level. Decreasing the gain K_i of the I-Part increases the amplitude of the response. The speed of the response could be increased by shortening the averaging time t . In our circuit for this purpose some resistors and capacitors had to be changed.

3.1.3 Derivative-Part

The I-Part is just reacting when the value is changing, as it can not forecast the future signal behavior. Therefore the D-Part is necessary. The Derivative-Controller is auguring the future behavior of the signal to solve this problem. Its output depends on the derivative of the error, the rate of change multiplied with the derivative constant K_d

$$y_d(t) = K_d \cdot \frac{de(t)}{dt}. \quad (3.3)$$

The speed of response could be increased by increasing the gain K_d of the D-Part. For the intensity stabilization the D-Part is not used, only the P- and I-Part are

necessary. In Figure 3.1 the three controller types and the functions of the complete PID are shown schematically. The final output of the PID is generated by combining all three output values.

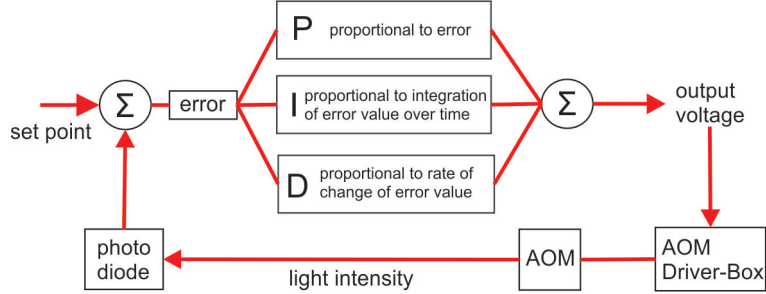


Figure 3.1: Scheme of the PID function. The three controller types operate with the error to generate a output signal which is fed back to the input signal.

3.2 Technical Setup

For the PID-Circuit an existing board was used. The original circuit was designed for frequency stabilization, for the purpose of intensity stabilization some modifications had to be done. This changes are described in the following paragraph.

3.2.1 Modified PID for Intensity Stabilization

The intensity stabilization operates on a different time scale than the frequency stabilization. For that reason, two of the capacitors in the circuit were changed. Figure B.1 and B.2 in the appendix show the original circuit diagram [21] with the necessary modifications for the intensity stabilization marked in blue and red.

Both of these capacitors are part of an integration amplifier in the circuit. Basically a integrator is a inverting amplifier, where the feedback resistor is replaced with an capacitor. Then the feedback is frequency dependent. The time constant of this integration is defined as [16]

$$\tau_i = R_1 \cdot C. \quad (3.4)$$

relating to the circuit diagram in Figure 3.2.

As described in the Basic Working Principle the speed of the I-Part can be increased by shortening the averaging time. For this purpose one 10 nF capacitor was changed to 47 pF, this decreases the time constant of that part by factor of $3.7 \cdot 10^{-3}$ according to equation (3.4). Besides, the wiring of the used slow output was modified by bypassing the OpAmp¹ with an 1 kΩ resistor and another 12 μF capacitor was changed to 47 nF. The bypass manages that the output is 5 V, when the error value is zero. The change of the second capacitor decreases the time constant by a factor of $4.5 \cdot 10^{-3}$. Through this changes, the PID is much faster, which is needed for the intensity stabilization. Figure 3.3 shows the performance of the P- and I-Part used separately with maximum gains K_p and K_i . Figure 3.3a illustrates that the P-Part

¹Operational Amplifier

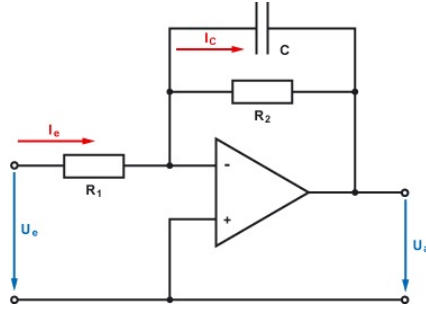


Figure 3.2: Circuit diagram of a basic Integrator OpAmp circuit, taken from [16]. In our case the speed of the integrators in the circuit was increased through changing the capacity C .

reacts with a phase shift to the signal changes. Relating to the fast increasing error and output signals, the constant K_p is set very high, which leads to oversteering. The same behavior could be observed in Figure 3.3b for the I-Part. Additionally the I-Part starts to oscillate temporary.

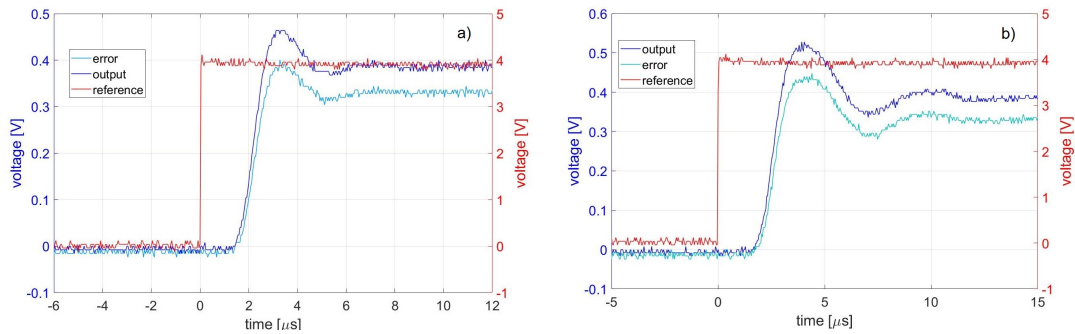


Figure 3.3: Performance of the Proportional (a) and Integrational Part (b) for max. K_p and K_i with the error and the output value in blue and the reference value in red. The voltage of the signals is displayed versus time.

The frequency limits of this PID board are illustrated in the Figure 3.4. If the PID works completely, the error value and the output value in blue should exactly follow the reference signal in red. The Figures show that the PID is too slow to control the signal for frequencies that high. That is illustrated with the fact that the edges of the blue signals are rounded in both pictures. Comparing, both figures shows that the phase shift of the output and the reference signal increases with higher frequencies. Through testing the performance of the PID we found out that the max. frequency it works stable is 130 kHz. Then the phase of the output signal starts to shift.

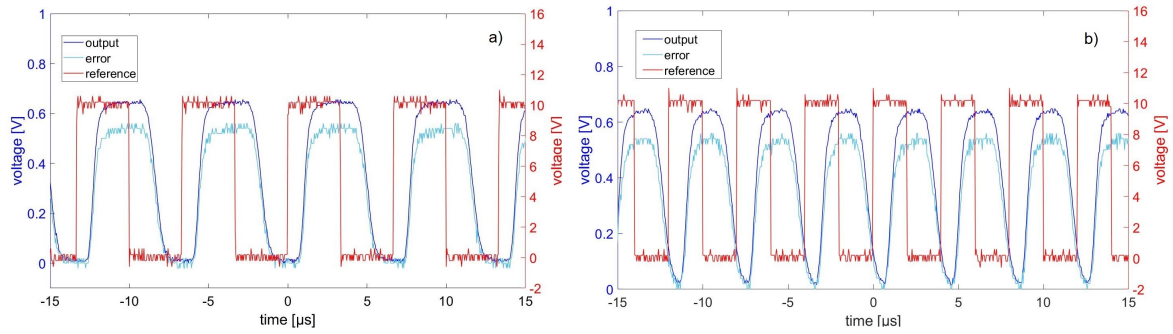


Figure 3.4: Limitation of the PIDs performance for high frequencies, here shown with a 150 kHz square function in a) and a 250 kHz in b). The error signal and the output are shown in blue, the reference signal in red. The voltage of the signals is displayed versus time. It can be mentioned that the output signal has a phase shift relating to the reference signal and comparing both plots the phaseshift increased with higher frequency.

3.2.2 Final Arrangement of the AOM and the PID to a Feedback Loop

After the different technical parts of the setup were finished, the AOM and the PID were put together to a feedback loop on the experiment table. The PID was first tested on an external desk before including it to the experiment. Therefore, a fiber supplied the beam from the AOM setup (Figure 2.6) to the setup for the final intensity stabilization presented in Figure 3.5 and 3.6. Firstly, the beam is sent through a $\lambda/2$ -waveplate and a polarizing beam splitter. Then, a beam sampler picks off 1 – 10% of the incident beam, using fresnel reflection. This less intense beam is sent to a photo diode which is connected to the PID controller.

The signal of the diode is the process value of the PID and the output of the PID is attached to the AOM-Driver-Box which then regulates the signal operating the AOM. By that the feedback loop is closed. Figures 3.7a) and b) present the intensity stabilization at the example of two different wavefunctions as reference. The error and the output signal of the PID in blue are exactly following the reference signal in red.

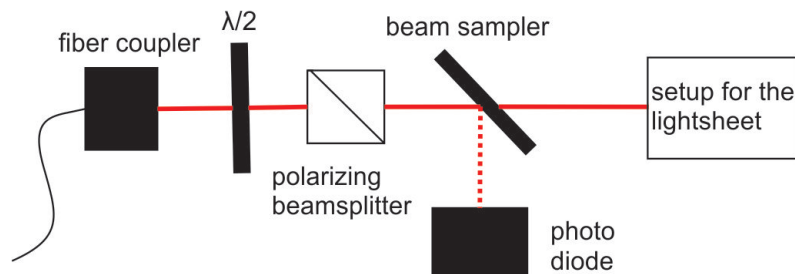


Figure 3.5: Sketch of the final setup for the intensity stabilization. The signal of the photodiode is sent to the PID, which then regulates the signal of the AOM.

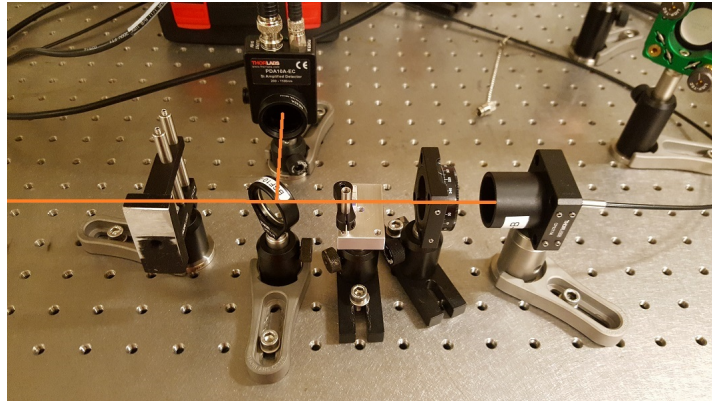


Figure 3.6: Built setup for the intensity stabilization. The diffracted beam from the AOM is guided by a fiber and then sent through a $\lambda/2$ -waveplate and a polarizing beamsplitter. A beam sampler picks up $\sim 1\%$ of the beam for the diode for the stabilization.

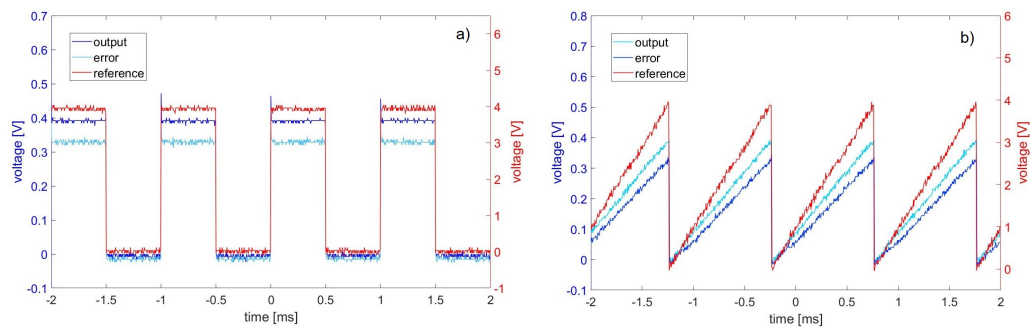


Figure 3.7: Test of the intensity stabilization with a square wave function (a) and a sawtooth function (b). On both Figures the reference signal is marked in red and the error and output values in blue. Displayed is the voltage of the signals in relation to the time. In this case the P-Part and I-Part are adjusted well and the output directly follows the reference signal.

Chapter 4

The Lightsheet

The field of laser trapping is of great interest for the work with ultracold gases, as it opened up new experimental possibilities. According to R.Grimm, M.Weidemüller and Y.B. Ochinnikov trapping methods "have very often served as the key to great scientific advantages, covering physics (...) of ultracold quantum matter." [1] Neutral atoms can be trapped (and cooled) based on three different principles, leading to radiation pressure traps, magnetic traps and optical dipole traps [1]. The lightsheet setup in this experiment is an optical dipole trap. For trapping neutral atoms, a Gaussian laser beam is focussed to a 'pancake' shape on the atoms. In the following sections the basics of Gaussian optics and optical traps are outlined.

4.1 Basic Working Principles

4.1.1 Gaussian Optics

Gaussian optics is a theoretical framework to describe the propagation of a lightfield in a laser mode. Generally laser beams can propagate in various spatial modes. The following equations are given for the TEM₀₀ mode of the laser, based on the references [1] and [4]. The intensity in this case is described as

$$I(r) = I_0 \cdot \exp\left(\frac{-2 \cdot r^2}{w(z)^2}\right) \quad (4.1)$$

with I_0 the maximum intensity at the optical axis and r the distance from it. The parameter w describes the beam waist defined as the distance from the axis where the intensity has fallen to $1/e^2$. Along the optical axis the beam width evolves according to

$$w(z) = w_0 \cdot \sqrt{1 + \left(\frac{\lambda \cdot z}{\pi \cdot w_0^2}\right)^2} = w_0 \cdot \sqrt{1 + \left(\frac{z}{z_R}\right)^2} \quad (4.2)$$

and the Rayleigh range is given by

$$z_R = \frac{\pi \cdot w_0^2}{\lambda}. \quad (4.3)$$

When the beam is focussed through a lens the new beam waist can be calculated with

$$w_f^2 = w_0^2 \frac{f^2}{z^2 + z_R^2} \quad (4.4)$$

where z is the position of the beam waist in front of the lens [19].

4.1.2 Optical Traps

The development of optical trapping opened up a great range of experimental possibilities for observing BECs¹. For example according to M.D.Barett *et al.* all-optical trapped BEC is "surprising simple and an order of magnitude faster than standard BEC experiments" which use magnetic traps [20]. Laser cooling and trapping enabled researchers to study ultracold quantum gases.

The lightsheet developed within this thesis, an optical dipole trap, is used for trapping atoms, not cooling. The following description of the theory of optical traps is based on the chapter "Optical Dipole Potential" in R.Grimms and M.Weidemüllers paper "Optical Dipole Traps for Neutral Atoms"[1].

Optical dipole traps are based on the electric dipole interaction of a detuned laser beam with the atoms. These type of traps offer a great variety of trap geometries and applications. For example the 'pancake' shaped light sheet developed in this case, is used to realize quasi two dimensional quantum gases.

Neutral atoms can be trapped in the focus of a laser field that is far red detuned from a strong optical transition. In general two types of detuning are used. Red-detuned traps catch the atoms in a intensity maximum. In contrast, blue-detuned traps catch them in an intensity minimum between two repulsive 'walls'.

The basic principle of an optical dipole trap is an induced dipole moment. The optical dipole force is a result of the dispersive interaction of the intensity of the laser beam with the induced dipole moment of the atoms. In the following, all derived equations are based on the assumption, that the atom, specifically the outermost electron, can be treated with a harmonic oscillator model.

When an atom is exposed to laser light the electric field of the light wave induces a dipole moment \mathbf{p} in the neutral atom, which oscillates at the driving frequency ω . Thereby, ω is the frequency of the light wave. In linear optics the strength of \mathbf{p} is proportional to the amplitude of the electric field $\hat{\mathbf{E}}$.

$$\hat{\mathbf{p}} = \alpha \hat{\mathbf{E}} \quad (4.5)$$

with α the specific polarizability of the medium, depending on ω .

Light is a temporally changing electromagnetic wave and can induce a dipole moment in media. Based on the dependence of the induced dipole moment with the electric field of the wave an interaction potential occurs

$$V = -\frac{1}{2} \langle \mathbf{p} \mathbf{E} \rangle. \quad (4.6)$$

¹Bose-Einstein-Condensate

Here $\langle \rangle$ denotes the average over one period of the light field. With equation 4.5 and the intensity $I(\mathbf{r}) = 2\epsilon_0 c |\hat{\mathbf{E}}|^2$ we find

$$V(\mathbf{r}) = -\frac{1}{2\epsilon_0 c} \Re(\alpha) I(\mathbf{r}). \quad (4.7)$$

The factor 1/2 points out, that the dipole moment is induced and not permanent. The dipole force is given by the gradient of the interaction potential

$$\mathbf{F}_{\text{dip}}(\mathbf{r}) = -\nabla V = \frac{1}{2\epsilon_0 c} \Re(\alpha) \nabla I(\mathbf{r}). \quad (4.8)$$

The power absorbed by the oscillator is given as

$$P_{\text{abs}} = \langle \dot{\mathbf{p}} \mathbf{E} \rangle = \frac{\omega}{\epsilon_0 c} \text{Im}(\alpha) I. \quad (4.9)$$

Here, the imaginary part of the polarizability describes the phase-delayed part of the oscillation. Using the wave-particle duality, the light can be described as photons with $E = \hbar\omega$ and the absorption can be treated by the picture of photon scattering with alternating absorption and re-emission. The appropriate scattering rate is given as

$$\Gamma_{sc}(\mathbf{r}) = \frac{P_{\text{abs}}}{\hbar\omega} = \frac{1}{\hbar\epsilon_0 c} \text{Im}(\alpha) I(\mathbf{r}). \quad (4.10)$$

For the next steps we assume that only a single atom is polarized by the electromagnetic wave. For identifying the polarizability of the atom we assume that the nucleus and the electron are harmonically bound as in the Lorentz model of a classical oscillator. In this case the eigenfrequency of this system is ω_0 . The equation of motion for the electron is then

$$\ddot{x} + \Gamma_\omega \dot{x} + \omega_0^2 x = -\frac{eE(t)}{m_e} \quad (4.11)$$

with the classical damping rate $\Gamma_\omega = \frac{e^2 \omega^2}{6\pi\epsilon_0 m_e c^3}$ on the basis of energy loss caused by radiation. For the polarizability α by integration of equation (4.11) follows

$$\alpha = \frac{e^2}{m_e} \frac{1}{\omega_0^2 - \omega^2 - i\omega\Gamma_\omega} \quad (4.12)$$

By substituting $\frac{e^2}{m_e} = \frac{6\pi\epsilon_0 c^3 \Gamma_\omega}{\omega^2}$ and using the damping rate $\Gamma \equiv \Gamma_{\omega_0} = \left(\frac{\omega_0}{\omega}\right)^2 \cdot \Gamma_\omega$ of the resonant case, the polarizability can be split in a real and imaginary part with

$$\alpha = 6\pi\epsilon_0 c^3 \frac{\Gamma/\omega_0^2}{\omega_0^2 - \omega^2 - i(\omega^3/\omega_0^2)\Gamma}. \quad (4.13)$$

For optical transitions ω_0 and ω are of the same order of magnitude. Consequently, the term $\left(\frac{\omega^3}{\omega_0^2}\right)^2 \Gamma^2$ can be neglected as it is much smaller than $(\omega_0^2 - \omega^2)^2$. In a second step the counter rotation term $(\omega_0 + \omega)^{-1}$ can be neglected.

Then the polarizability can be simplified to

$$\alpha = 6\pi\epsilon_0 c^3 \left(\frac{1}{2\omega_0^3} \left(\frac{\Gamma}{\omega_0 - \omega} + \frac{\Gamma}{\omega_0 + \omega} \right) - i \frac{1}{4\omega_0^2} \left(\frac{\omega}{\omega_0} \right)^3 \left(\frac{\Gamma}{\omega_0 - \omega} + \frac{\Gamma}{\omega_0 + \omega} \right)^2 \right) \quad (4.14)$$

$$\approx 6\pi\epsilon_0 c^3 \left(-\frac{1}{2\omega_0^3} \left(\frac{\Gamma}{\Delta} \right) + i \frac{1}{4\omega_0^2} \left(\frac{\Gamma}{\Delta} \right)^2 \right) \quad (4.15)$$

with the laser detuning $\Delta = \omega - \omega_0$. Assuming $\frac{\omega}{\omega_0} \approx 1$ and $|\Delta| \ll \omega, \omega_0$, the dipole potential can be finally written as

$$V(\mathbf{r}) = \frac{3\pi c^2}{2\omega_0^3} \frac{\Gamma}{\Delta} I(\mathbf{r}). \quad (4.16)$$

The pre-factor can be positive or negative, depending on the sign of the detuning Δ . For red-detuned light is $\Delta < 0$ and the minimum of the potential is at the maximum of the intensity. In this case the trap has a attractive potential. Furthermore, the scattering rate can now be simplified to

$$\Gamma_{sc}(\mathbf{r}) = \frac{3\pi c^2}{2\hbar\omega_0^3} \left(\frac{\Gamma}{\Delta} \right)^2 I(\mathbf{r}). \quad (4.17)$$

As equation (4.16) illustrates, the potential depth is scaling with $\frac{1}{\Delta}$. In contrast the scattering rate in (4.17) scales with $\frac{1}{\Delta^2}$. For optical traps the scattering rate should be kept as low as possible, to not loose too many atoms of the sample. Therefore, far detuned lasers are used as the scattering rate drops much faster than the potential.

4.2 Final Setup for the Lightsheet

After the setup for the intensity stabilization was finished and tested, the optical elements were arranged to create the desired optical potential. A quasi two-dimensional potential is realized with cylindrical lenses, as this lenses focus the beam only in one direction. For this reason, the focus of cylindrical lenses is elliptical, which is necessary to create a flat light sheet.

The basic parts of the sheet are illustrated in Figure 4.1 and Figure 4.2 shows the first test setup. On the right side it shows the arrangement for the intensity stabilization, which was shown more detailed in Figure 3.6. All lenses are chosen in consideration of the required beam waist of the light sheet. Therefore the ratio of the cylindrical lenses is chosen depending on the focal length of the spherical length, as the beam waist in front of a lens determines the waist behind the lens according to equation (4.4).

Directly behind the beam sampler the laser beam passes the first cylindrical lens. The two cylindrical lenses form a telescope to provide the desired shape and size of the lightsheet. Due to limited space at the experiment table a lens with a negative focal length of $f_1 = -60$ mm is used in combination with a $f_2 = 500$ mm lens, resulting in an aspect ratio of the beam of 1 : 8.3. The distance between those lenses

results from the focal length of both as $d = f_1 + f_2 = 440$ mm. Those should be adjusted well, to ensure that the beam is collimated afterwards. Finally, the sheet is created with a spherical lens. Due to given circumstances the distance of this lens and the sample is 20 cm, therefore a lens with $f = 200$ mm is chosen.

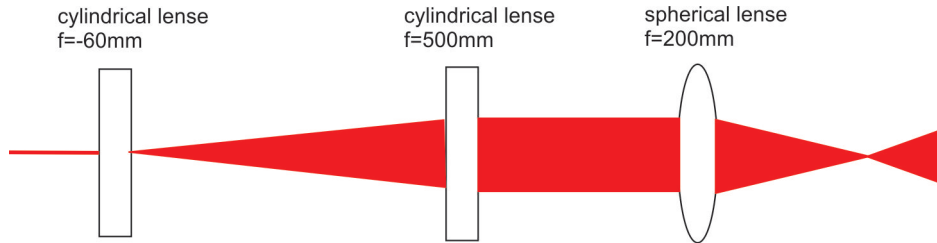


Figure 4.1: Sketch of the arrangement of the lenses for generating the lightsheet. The magnification of the telescope is chosen in consideration of the desired waist of the lightsheet along the short axis.

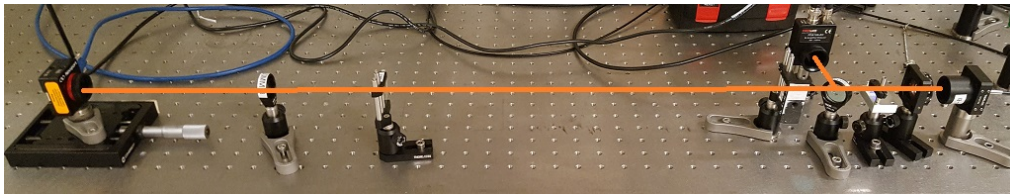


Figure 4.2: Arrangement of all optical components for the lightsheet. After the intensity stabilization setup at the right side the beam passes two cylindrical lenses and a spherical lens. The sheet appears at the position of the camera on the left side.

With this setup the beam waist along the short and long axis of the elliptical beam was measured as a function of the position z along the optical axis. For this measurement the position of the beam profiler, visible on the left side of figure 4.2 was varied along the z -axis. The results are shown in Figure 4.3 and 4.4. With equation 4.2 used as fit, a waist of $\omega_0 = 10.1(\pm 2.0) \mu\text{m}$ along the short axis was measured. Along the long axis, $\omega_0 = 110.7(\pm 5.9) \mu\text{m}$ was measured. In contrast to the expected aspect ratio, we determine it to 1 : 10.

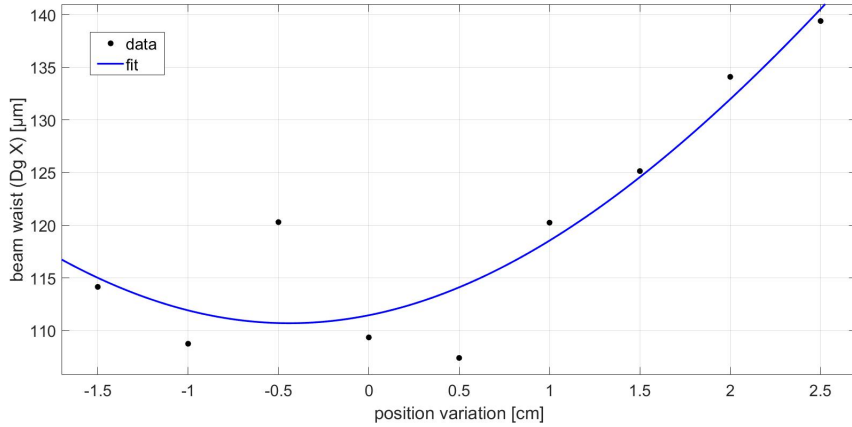


Figure 4.3: The beam waist in x-direction, when moving the beam profiler along the z -axis. Shown is the beam waist as a function of the position change. The blue line is a fit to the data based on equation (4.4).

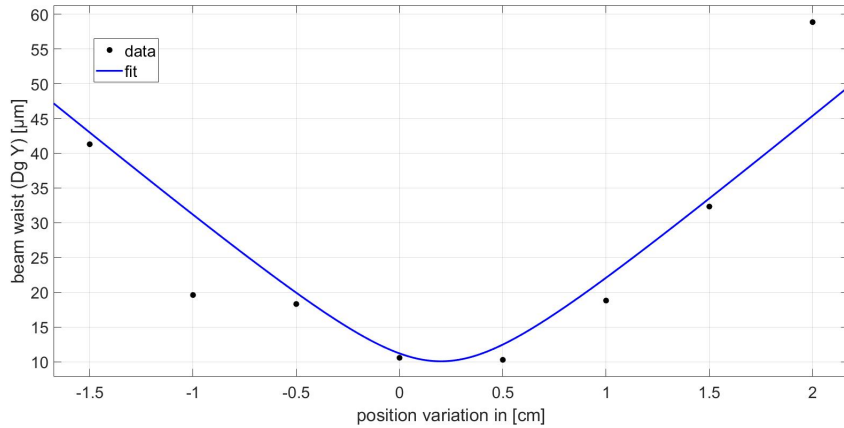


Figure 4.4: The beam waist in y direction when, moving the beam profiler along the z -axis. Shown is the beam waist as a function the position change. The blue line is a fit to the data based on equation (4.4).

Finally, the stabilization setup and the lightsheet were both included into the main experiment. Figure 4.5 shows the final setup as it is now used in the experiment.

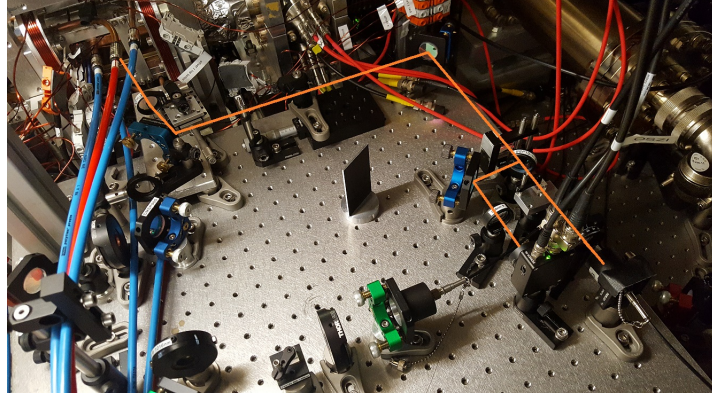


Figure 4.5: Picture of the lightsheet setup included into the experiment, with the path of the beam marked in orange. The beam is guided through a fiber, then passes the stabilization setup on the right side. Afterwards, it passes the lightsheet arrangement. The sheet is finally generated inside the chamber with the sample (left corner).

4.3 Quantifying the Trap Frequency of the Lightsheet

4.3.1 Theoretical Calculation

First, the trap frequency is calculated out of the given parameters and then compared with the experimental result. For this calculation, the theoretical beam waist of the lightsheet is needed. This calculation is based on the theory of the Gaussian Beam. For this purpose first the Rayleigh length of the beam after the fiber has to be calculated

$$z_R = \frac{\pi \cdot w_0^2}{\lambda} = \frac{\pi \cdot (2.5\mu\text{m})^2}{855.21\text{ nm}} = 22.96\ \mu\text{m} \quad (4.18)$$

with $w_0 = 2.5\ \mu\text{m}$ the radius of the fiber core and $\lambda = 855.21\text{ nm}$ the wavelength of the stabilized laser beam. With this result and the effective focal length ($f = 8.00\text{ mm}$) of the aspheric lens (Thorlabs A240TM-B) of the fiber coupler, the new beam waist after the coupler can be calculated

$$w_f^2 = w_0^2 \cdot \frac{f^2}{z_R^2} = (2.5\mu\text{m})^2 \cdot \frac{(8\text{ mm})^2}{(22.96\ \mu\text{m})^2} = 0,756\text{ mm}^2 \quad (4.19)$$

$$\Rightarrow w_f = 0.87\text{ mm}. \quad (4.20)$$

After that, the beam is sent through two cylindrical lenses with $f_1 = -60\text{ mm}$ and $f_2 = 500\text{ mm}$ and a spherical lens with $f_3 = 200\text{ mm}$. As the lightsheet has an

elliptical geometry, we calculate the waists in x- and y-direction via

$$w_{0,x} = \frac{\lambda \cdot f_3}{\pi \cdot w_f} = 62.6 \mu\text{m} \quad (4.21)$$

$$w_{0,y} = \frac{\lambda \cdot f_1 \cdot f_3}{\pi \cdot f_2 \cdot w_f} = 7.51 \mu\text{m}. \quad (4.22)$$

Comparing this values with the measured waists from the Figures 4.3 and 4.4 we find, that the measured waist in x-direction is 70.4% bigger than the calculated waist. For the waist along the y-axis the measured waist is 40.5% bigger than the calculated one. This huge difference can be explained with the difference between fiber core size and waist of the light mode inside. With these calculated waists, one can now calculate the theoretical trap frequency. The trap frequency along the long axis is given by

$$\omega_x = \sqrt{\frac{4 \cdot V_0}{m \cdot w_{0,x}^2}}. \quad (4.23)$$

The amplitude of the potential can be calculated with

$$V_0 = \frac{\Re(\alpha)P}{\epsilon_0 \pi c w_{0,x} \cdot w_{0,y}} \quad (4.24)$$

with $P = 100 \text{ mW}$ and

$$\Re(\alpha) = 6\pi\epsilon_0 c^3 \left(-\frac{1}{2\omega_0^3} \cdot \frac{\Gamma}{\Delta} \right). \quad (4.25)$$

The D-Line of Rb^{87} has two Finestructure states D_1 ($5^2S_{1/2} \rightarrow 5^2P_{1/2}$) and D_2 ($5^2S_{1/2} \rightarrow 5^2P_{3/2}$). The wavelengths of the transitions are $\lambda_1 = 795 \text{ nm}$ and $\lambda_2 = 780 \text{ nm}$, therefore the detuning is in both cases nearly equal. Other transitions are not relevant, for example the transitions to $6^2P_{1/2}$ or $6^2P_{3/2}$ take place at 421 nm and 420 nm , which leads to a much higher detuning Δ and a smaller polarizability α . On this reason only one frequency is measured, but both lines have to be taken to account. The effective transition frequency ω_{eff} and the effective scattering rate Γ_{eff} can then be calculated with

$$\omega_{\text{eff}} = \frac{1}{3}\omega_1 + \frac{2}{3}\omega_2 \quad (4.26)$$

and

$$\Gamma_{\text{eff}} = \frac{1}{3}\Gamma_1 + \frac{2}{3}\Gamma_2 \quad (4.27)$$

using the parameters given in table 4.1.[4] Now, with the results $\omega_{\text{eff}} = 2\pi \cdot 381.856 \text{ THz}$

Line	Frequency ω_0	Decay Rate Γ
D_1	$2\pi \cdot 377.107 \text{ THz}$	$2\pi \cdot 5.746 \text{ MHz}$
D_2	$2\pi \cdot 384.23 \text{ THz}$	$2\pi \cdot 6.065 \text{ MHz}$

Table 4.1: Parameters for calculating the effective frequency and scattering rate[2].

and $\Gamma_{\text{eff}} = 2\pi \cdot 5.959 \text{ MHz}$ the real part of the polarizability $\Re(\alpha) = 3.144 \cdot 10^{-38} \frac{\text{C}}{\text{V}} \cdot \text{m}^2$

is calculated. This leads to potential depth of $V_0 = 8.02 \cdot 10^{-28} \text{J}$. Finally the trap frequency can be calculated with equation 4.23 leading to

$$\omega_T = 19853.1 \text{ Hz} \quad (4.28)$$

$$\Rightarrow f_T = 3159.7 \text{ Hz} \quad (4.29)$$

4.3.2 Analysis of an Exemplary Measurement

The following measurements of the trap frequency were taken with the final setup, after adjusting the lightsheet.

To get the frequency, the lightsheet was slowly linearly ramped within 200 ms to the full intensity of 100 mW. Then the intensity was briefly reduced to 30 mW for one millisecond and then set back to 100 mW. Through this the oscillation of the cloud of atoms in the lightsheet was kickstarted. As the amplitude of the potential is oscillating, one does not excite the basic vibration mode but the next higher vibration mode. Then the cloud oscillates at twice the trap frequency. For this mode the atom cloud pulses, it expands and tightens periodically. This is measured by taking pictures of the cloud at different hold times after the kick, in $50 \mu\text{s}$ steps between 0 and 2 ms.

For illustrating this vibration two pictures of the measurements are shown in Figure 4.6, with $200 \mu\text{s}$ between both pictures.

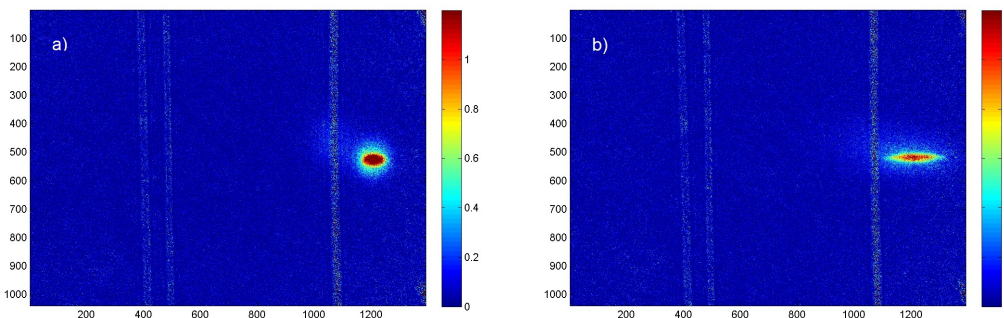


Figure 4.6: Pictures of the atom cloud taken with $200 \mu\text{s}$ between both images. Compared to picture a) the cloud has expanded in picture b) in x-direction

The data was recorded with absorption imaging. The measured data is given in three different files, one with the atom cloud x_1 , one without atoms x_2 and one background image x_3 . In consideration of the Beer-Lambert law, the data needed for identifying the trap frequency is extracted from these files through calculating the logarithm pixelwise

$$x = -\log\left(\frac{x_1 - x_3}{x_2 - x_3}\right). \quad (4.30)$$

The trap frequency could be extracted from the time evolution of the horizontal width of the atom cloud. One way to get the width is to search for the maximum value of the data and to fit a Gaussian function to the row including this value. The

fitted function is given by

$$f(x) = a \cdot \exp\left(-\left(\frac{x-b}{c}\right)^2\right) \quad (4.31)$$

where the fit-parameter c gives us the width of the cloud. As there are four repetitions of the measurement done, for every wait time four width values exist. For the calculation of the trap frequency the average of this four measurements was used. The standard derivation of them is used as errorbars to the graph in Figure 4.7. Then this averaged width values were plotted over time and a damped sinus given by

$$g(x) = a \cdot \exp(-\delta x) \cdot \sin(\omega x + d) + e + f x \quad (4.32)$$

was fitted to the data. The extracted frequency ω is twice the trap frequency as stated above.

From these considerations, we find $f_T = \frac{1}{2} \frac{\omega}{2\pi} = 1363(\pm 8)$ Hz, measured at a power of 100 mW. This is less than half of the value of the theoretically calculated trap frequency. But the theoretical result does not represent the real conditions, as it used the calculated beam waist of the lightsheet. The real waist differs from the theory as the optical parts have limited accuracy. Furthermore the position of the sample in the sheet is relevant, the sample could not be perfectly in the focus of the beam. Therefore the real waist of the lightsheet is not the above calculated minimum waist.

A better value for comparing the frequencies gives a calculation with the measured waists $w_{0,x} = 10.1(\pm 2) \mu\text{m}$ and $w_{0,y} = 110.7(\pm 5.9) \mu\text{m}$. In this case the potential is $V_0 = 3.37(\pm 0.7) \cdot 10^{-28}$ J and with this result the trap frequency is $f_T = 1523.5(\pm 376)$ Hz. This result points the dependency of the trap frequency and the beam waist out.

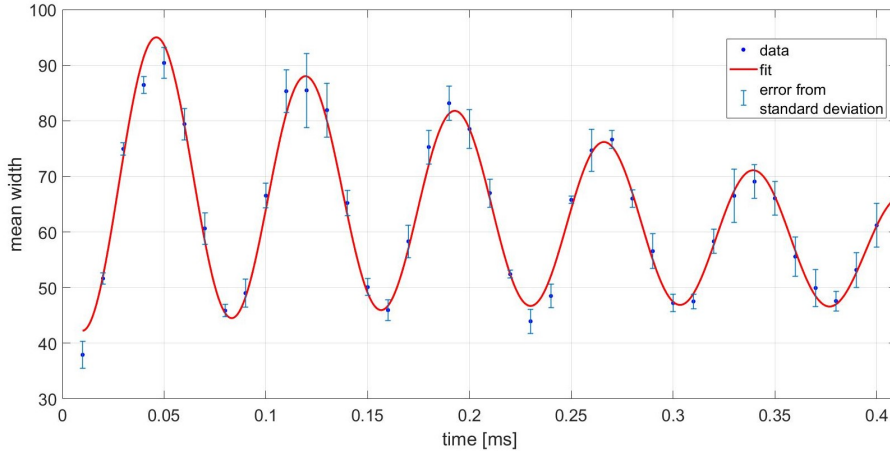


Figure 4.7: Time evolution of the horizontal width of the cloud averaged over 4 experimental realizations. The data is plotted with blue dots and the standard deviation as errorbars. The red line shows the fitted function. As expected the width follows a damped sinusoidal function, with the double of the trap frequency.

Chapter 5

Conclusion and Outlook

The aim of this thesis was to build a setup for a lightsheet which provides two-dimensional confinement. On this purpose a optical setup for shaping the laser beam and a feedback loop for intensity stabilization were constructed. The setup for the feedback loop included an AOM (Crystal Technology, type 8020-125) with a self-built Driver-Box and a modified PID-Controller. The AOM operates at 80 MHz and needs min. 1.5 W (=31.76 dBm) power. Therefore a Driver-Box was built to generate a suitable signal for operating the AOM. Measuring the output signal for 80 MHz the Box provides ca.32 dBm at every channel. Then the first part of the setup was put together and the AOM was integrated to the path of a 855 nm laser beam. In this context an diffraction efficiency of up to 80% was viable. Second, a PID originally designed for frequency stabilization, was modified for intensity stabilization. Therefore the operating speed of the PID was increased through exchanging two capacitors. This configuration is fast enough for signals up to ca. 130 MHz. Afterwards, the PID was connected with the Driver-Box of the AOM to stabilize the beam intensity, before sending it to the lightsheet arrangement. Finally, the optical setup for the sheet was constructed with two cylinder lenses with $f_1 = -60$ mm and $f_2 = 500$ mm and one spherical lense with $f_3 = 200$ mm. This last lens creates the lightsheet and is chosen in consideration of the distance of the setup to the sample. In a last step the trap frequency of the trap was measured, by imaging the oscillation of an atom cloud oscillating in the lightsheet. The frequency extracted of the data is $f = 1363(\pm 8)$ Hz.

In conclusion it can be claimed that the aim of the thesis was fulfilled, as the lightsheet is now used in the experiment.

Nevertheless, as the lightsheet provides two-dimensional confinement, it could only be used together with the magnetic trap established in the experiment, because it does not hold the cloud stable along the propagation axis of the beam. Therefore, the next step is to build a crossed optical trap, by adding a second beam. This beam will be constructed with a 1064 nm laser. To prepare this the AOM-Driver-Box, built as part of this thesis, was constructed with four channels, to provide the possibility to add this second setup without significant effort. With a crossed trap the sample could be held in shape without the magnetic trap.

Appendix A

AOM

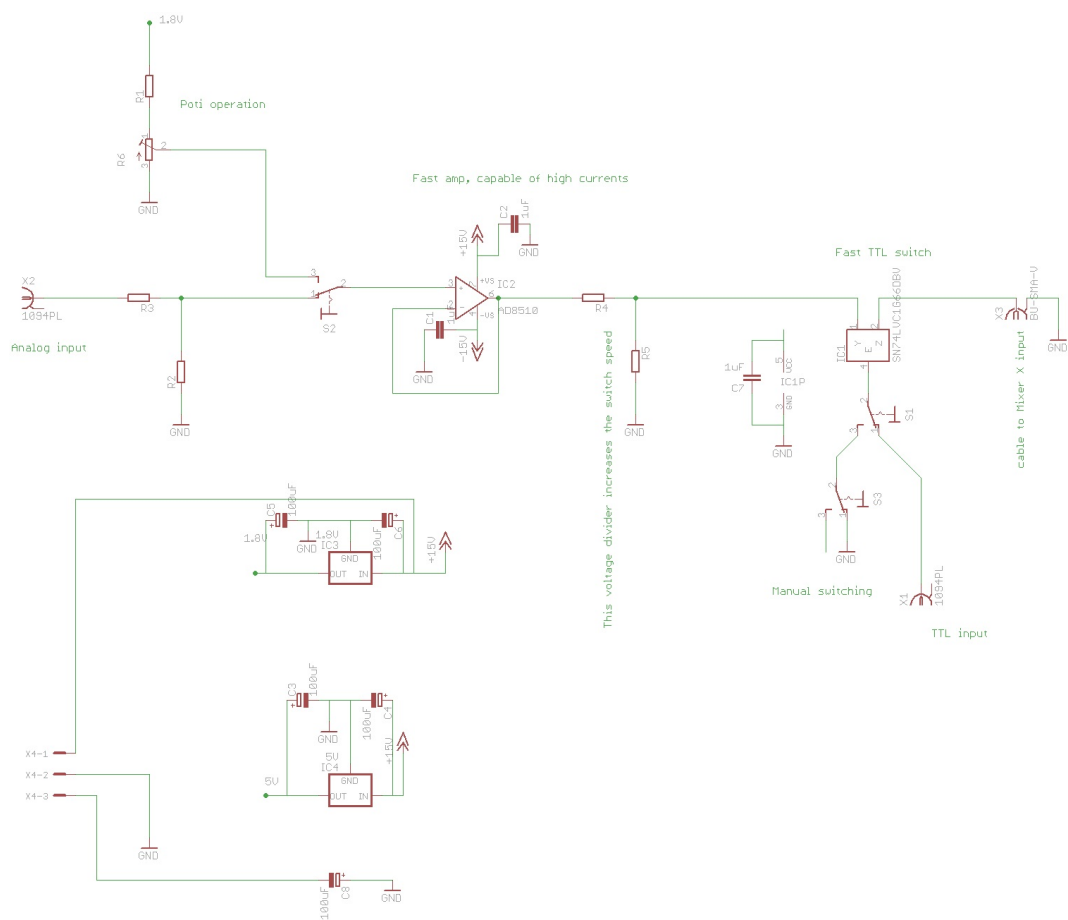


Figure A.1: Circuit diagram of one channel of the frontpanel electronics. *Source:* [20]

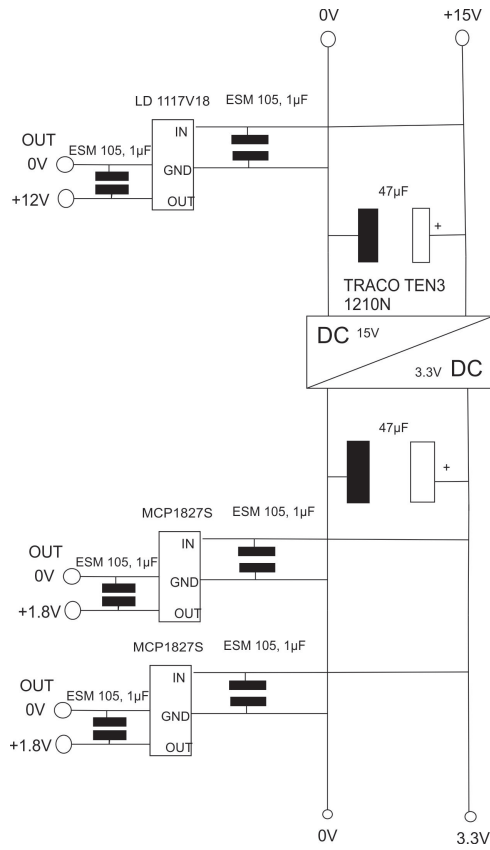


Figure A.2: Circuit diagram of the power supply for the AOM-Driver-Box

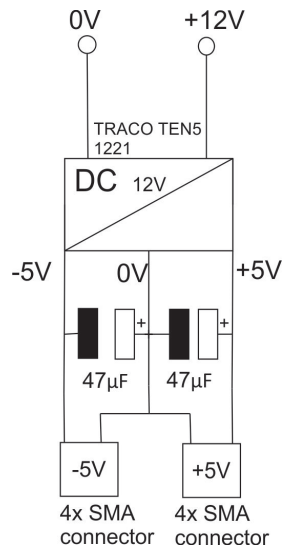
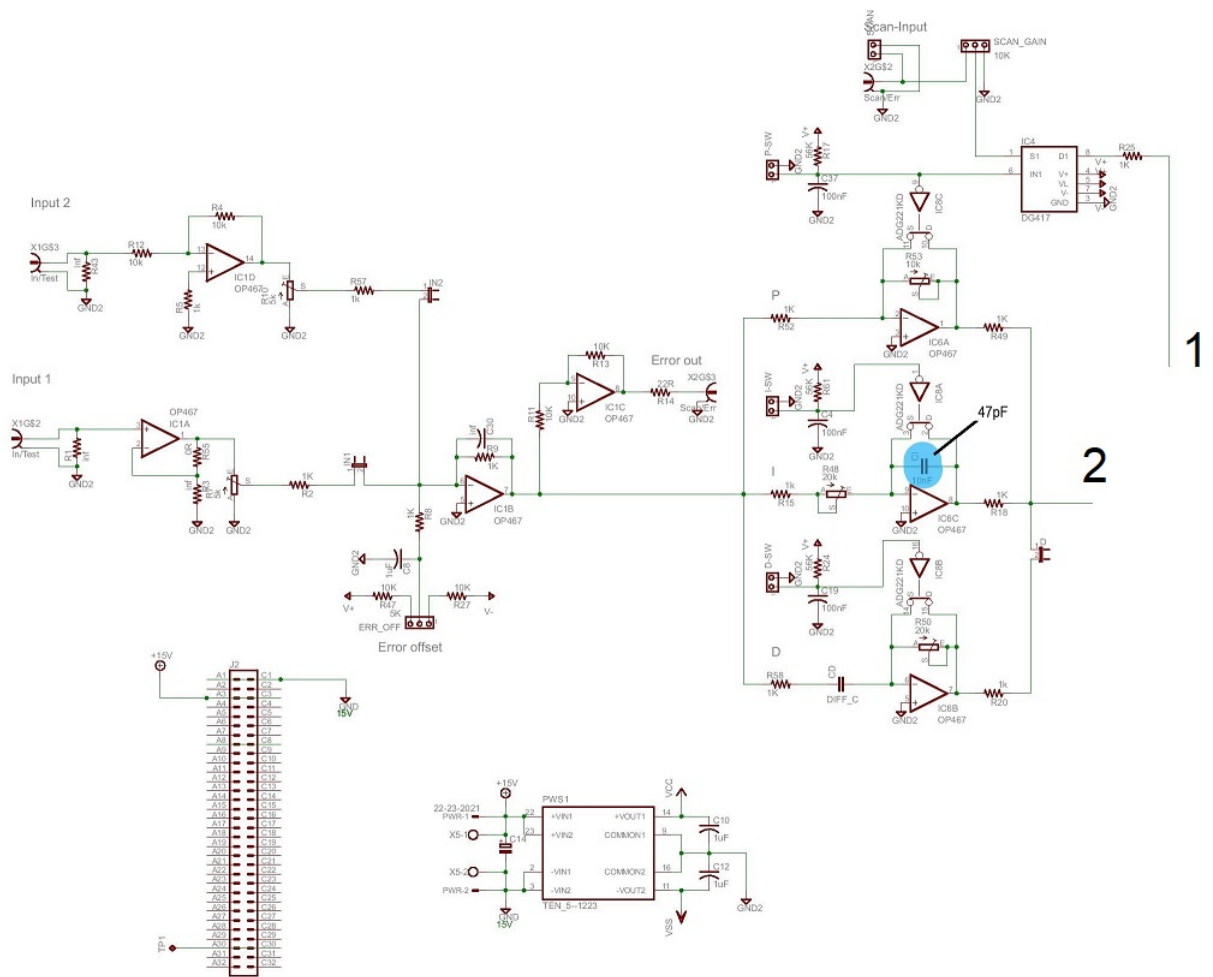


Figure A.3: Circuit diagram of the power supply with SMA connectors for the TTL switches

Appendix B

PID



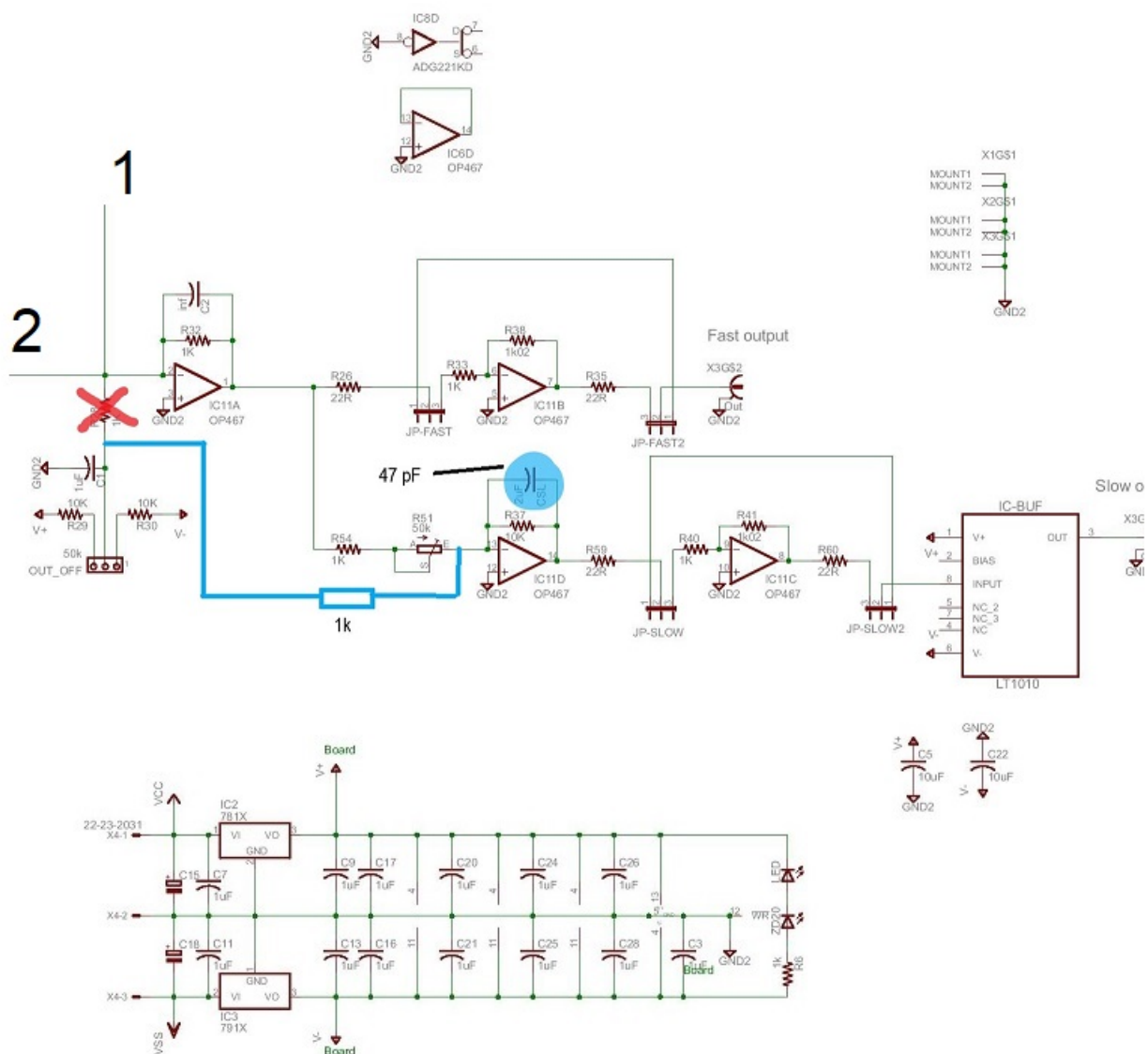


Figure B.2: Second part of the circuit diagram of the PID. Both parts are connected at 1 and 2. *Source:*[21]

References

- [1] R.Grimm, M.Weidemüller, Y.B.Ovchinnikov, *Optical dipole traps for neutral atoms*, Advances in Atomic, Molecular and Optical Physics Vol.42, 95-170 (2000), p.2-4, p.11, p.15
- [2] D.A.Steck, *Rubidium 87 D Line Data*, available at <http://steck.us/alkalidata>
- [3] M.T.Schlagmüller, *A single Rydberg Atom interacting with a Dense and Ultracold Gas*, Phd thesis (2015), p.126
- [4] M.Gustavsson, *A quantum gas with tunable interactions in an optical lattice*, Phd thesis (2008), p.41-42
- [5] Picture taken from the wiki-page of the 5th Institute of Physics
https://intern.pi5.physik.uni-stuttgart.de/mediawiki/index.php/File:AOM_driver.png
- [6] https://www.rp-photonics.com/acousto_optic_modulators.html accessed 06.12.2017
- [7] <http://www.acoustooptic.com/acousto-optic-principles.html> accessed 30.11.2017
- [8] http://www.pi5.uni-stuttgart.de/lectures/88/Versuch_AOM_Anleitung.pdf accessed 30.11.2017
- [9] Data Sheet AOMO 3080-125, Crystal Technology, available at https://goochandhousego.com/wp-content/pdfs/3080_125_97_01598_01rC.pdf
- [10] AD9959/PCB Evaluation Board Manual, available at http://www.analog.com/media/cn/technical-documentation/evaluation-documentation/57418637811849ADpcb_0.pdf
- [11] MiniCircuits SMA Mixer, available at <https://www.minicircuits.com/WebStore/dashboard.html?model=ZP-1LH-S%2B>
- [12] MiniCircuits TTL switch, available at <https://www.minicircuits.com/WebStore/dashboard.html?model=ZASWA-2-50DR%2B>

- [13] MiniCircuits Broadband Amplifier, available at <https://www.minicircuits.com/WebStore/dashboard.html?model=ZX60-6013E-S%2B>
- [14] MiniCircuits Broadband Amplifier, available at <https://www.minicircuits.com/WebStore/dashboard.html?model=ZHL-3A-S%2B>
- [15] Traco DC/DC Converter, available at <https://www.tracopower.com/products/ten5.pdf>
- [16] <https://www.elektronik-kompodium.de/sites/slt/0412061.htm> accessed 07.12.2017
- [17] <https://www.elprocus.com/the-working-of-a-pid-controller/> accessed 07.12.2017
- [18] https://www.rp-photonics.com/focal_length.html accessed 07.12.2017
- [19] M.D.Barett, M.-S.Chang, C.Hamley, K.Fortier, J.A.Sauer, M.S.Chapman, *All-Optical Atomic Bose-Einstein-Condensates*, published in *Proceedings of the XVII International Conference on Atomic Physics* p.31-38, ICAP 2002
- [20] Circuit diagram of the front panel electronics taken from the wiki-page of the 5th Institute of Physics, https://intern.pi5.physik.uni-stuttgart.de/mediawiki/index.php/File:Aom_board_scheme.png
- [21] Circuit diagram of the PID taken from the wiki-page of the 5th Institute of Physics, <https://intern.pi5.physik.uni-stuttgart.de/mediawiki/images/Schematic-PID-V32.pdf>
- [22] http://www.mt-berlin.com/frames_ao/descriptions/ao_effect.htm accessed 16.12.2017
- [23] https://www.csimn.com/CSI_pages/PIDforDummies.html accessed 16.12.2017